이학박사학위논문

Computational study of hydrogen storage in graphite derived nanomaterials

계산과학방법을 이용한 흑연 유도된 나노물질의 수소저장 연구

2016년 2월

서울대학교 대학원
물리천문학부
배재현

Computational study of hydrogen storage in graphite derived nanomaterials

계산과학방법을 이용한 흑연 유도된 나노물질의 수소저장 연구

지도교수 교수님

이 논문을 이학박사 학위논문으로 제출함

2016년 2월

서울대학교 대학원

물리천문학부

배재현

배재현의 박사 학위논문을 인준함

2016년 2월

위 원 장	위 원 장	(인)
부위원장	부 위 원	(인)
위 원	교 수 님	(인)
위 원	교 수 님	(인)
위 원	교 수 님	(인)

Computational study of hydrogen storage in graphite derived nanomaterials

Jaehyun Bae

Supervised by

Associate Professor **Jisoon Ihm**

A Dissertation

Submitted to the Faculty of

Seoul National University

in Partial Fulfillment of

the Requirements for the Degree of

Doctor of Philosophy

Feb. 2016

Department of Physics and Astronomy

The Graduate School

Seoul National University

Abstract

Computational study of hydrogen storage in graphite derived nanomaterials

Jaehyun Bae
Department of Physics and Astronomy
The Graduate School
Seoul National University

Hydrogen has long been considered as the energy carrier of the future. However, storage hydrogen efficiently and safely have been considered as a major obstacle in realizing hydrogen energy at present. In this thesis, we investigate the equilibrium of interacting gas molecules under the external potential, and propose a new hydrogen storage material derived from graphite using *ab initio* electronic structure calculation and grand canonical Monte-Carlo method.

Firstly, based on the simple thermodynamics, diffusive equilibrium under the external potential, we show that hydrogen molecules can be highly concentrated in the attractive potential well in the ambient conditions. Hydrogen molecules are vigorously move inside the potential well and retain gas from, it is very distinct feature of our storage mechanism compare with

storage mechanism based on the bonding at specific sites through Kubas interaction using transition metal atoms. As a realization, we propose a potassium intercalated graphite oxide as a scaffold material and show that relatively uniform potential well arises inside the layer and its strength is as large as 0.12eV. The enhancement of binding energy can be attributted to the induced dipole interaction from electric field generated by oxygen atom and potassium ion and small orbital hybridization. Room temperature hydrogen storage capacity is obtained by grand canonical Monte-Carlo simulation. The general trend of storage capacity with different chemistry of scaffold material is explained by equilibrium condition and density enhancement by the attractive potential.

Secondly, we study the energetics involved hydrogen confinement process. Isosteric heat of adsorption is one of the key quantities in the hydrogen storage experiment, and can be considered as a change of the enthalpy of adsorption process. In order to account the intermolecular interaction, we employed the cluster expansion method for interacting gas and analytically derived the equilibrium condition, which is valid in the ambient condition. The strength of the potential well as well as the interaction energy is reflected in the isosteric heat. This result can be applied to explain the physics of hydrogen storage using potential well.

We end up with summary and perspectives to be investigated more.

Keywords : hydrogen storage, graphite, graphite oxide, functional group, potential well, denstiy enhancement, density functional theory, Monte-Carlo

simulation

Student Number : 2008-20434

Contents

List of Figures

List of Tables

Chapter 1

Introduction

Hydrogen has been considered to be a clean and sustainable future energy source [1], but storing hydrogen safely and efficiently at ambient condition is the major obstacle for the commercializing fuel-cell powered vehicles. Hydrogen storage using Metal or chemical hydrides is one of the eldest and frequently studied method and shows high storage capacity [2], but storage material of this kind does not satisfy the requirements for the fast kinetics and reversibility. With current nanotechnology being developed, it is possible to synthesize nanoscale materials which have large surface area. Metal-organic frameworks (MOFs) is one of the representative material of this category and have been regarded as a promising storage materials owing to its porosity, fast kinetics, and the reversibility [3, 4]. However, high pressure and cryogenics are necessary in the adsorption process because of weak binding energy between hydrogen molecule and MOFs mainly via van der Waals interaction. People found that optimal binding energy for the ambient condition storage is realizable by introducing transition-metal (TM) atom into MOFs [5, 6]. TM atoms bound to the linker part of MOFs and H_2 molecule in the molecular form adsorbed to TM atoms via the so-called Kubas interaction [7]. Because of high cohesive energy and reactivity, TM atom clustering and contamination by other gas molecules hinder from experimental realization of storage density satisfying the DOE goal by the year

of 2020.

Along with rapid development of computer technology, computational material design have become a important part of the material researches. In this thesis, we study hydrogen storage of graphite derived nanomaterials and suggest a new storage mechanism using first-principles calculations based on density functional theory and multi-scale computational techniques.

First, we showed that gas storage in the potential well is conceptually different from gas storage using particular binding sites. Not only is thermodynamics equilibrium condition of two mechanism different, but also desired material properties for efficient storage are different. As a realization of potential for hydrogen molecules, potassium intercalated graphite oxide is chosen for the backbone material. We found that relatively uniform potential arises in between layers and investigated origin of the enhancement of potential energy. Room temperature storage capacity is obtained by performing Monte Carlo simulation, because of inter molecular interaction is crucial in the high pressure.

Second, we studied thermodynamics involved during the hydrogen storage in the potential well. We derived a formalism for the isosteric heat of potential confinement. In this derivation, we used the van der Waals equation to describe the intermolecular interaction.

The organization is as follows. In Chapter 2, computational techniques used in the thesis are briefly introduced. In Chapter 3, hydrogen storage capacity of potassium intercalated graphite oxide is investigated by using multiscale computational techniques. In Chapter 4, thermodynamics in the storage process is analyzed. Finally, all results are summarized in Chapter 6

with brief prospect.

Chapter 2

Computational Methods

2.1 Density Functional Theory

In principle, all physical and chemical properties of condensed matter can be obtained by solving Schrödinger equation of multi-particle (electrons and nuclei) system. (For the complete description, we need to take into account both electronic and nucleic degrees of freedom, but in this part, we only consider electronic degrees of freedom.)

In practice, however, solving multi-electron Schrödinger equation for the ground state of small molecular system needs tremendous computational costs. This stems from electron-electron interaction and statistics of many electrons, many methods are developed to calculate the effect of electron-electron interaction on electronic structure of material.

A groundbreaking work by Hohenberg and Kohn(HK) and Kohn and Sham(KS) paves new ways of describing interacting electrons system. In work, electron density rather than wavefunction is the basic variable, and ground state energy of system is given by functional of electron density. This idea was first adapted by Thomas and independently Fermi (TF), but solid mathematical formulation of theory is proved by HK and summarized by two theorems ;

2.1.1 Hohenberg-Kohn Theorem

Theorem 1 The external potential is a unique functional of electron density n(r), apart from a trivial additive constant [8].

Proof *reducio ad absurdum*. Suppose that there are two different external potential V_1 and V_2 which differ by additive constant and which lead to the same ground state electron density $n(\vec{r})$. The two external potential lead to two different Hamiltonians H_1 and H_2, which have different ground state wavefunction ψ_1 and ψ_2, which are supposed to have the same ground state electron density $n_0(\vec{r})$. Since ψ_2 is not the ground state of H_1, it follows that

$$E_1 = \langle \psi_1 \mid H_1 \mid \psi_1 \rangle < \langle \psi_2 \mid H_1 \mid \psi_2 \rangle \tag{2.1}$$

The strict inequality follows if the ground state is non-degenerated. The proof can readily be extended to degenerated case, which is out of interest here. The last term in Equation 2.1 can be written

$$\begin{aligned} \langle \psi_2 \mid H_1 \mid \psi_2 \rangle &= \langle \psi_2 \mid H_2 \mid \psi_2 \rangle + \langle \psi_2 \mid H_1 - H_2 \mid \psi_2 \rangle \\ &= E_2 + \int d\vec{r}[V_{ext,1}(\vec{r}) - V_{ext,2}(\vec{r})]n_0(\vec{r}), \end{aligned} \tag{2.2}$$

so that

$$E_1 < E_2 + \int d\vec{r}[V_{ext,1}(\vec{r}) - V_{ext,2}(\vec{r})]n_0(\vec{r}). \tag{2.3}$$

On the other hand, if we consider E_2 in exactly the same way, we find the same equation with interchanged subscript 1 and 2,

$$E_2 < E_1 + \int d\vec{r}[V_{ext,2}(\vec{r}) - V_{ext,1}(\vec{r})]n_0(\vec{r}). \tag{2.4}$$

Now, if we add Equation 2.3 and Equation 2.4, we arrived at the contradictory $E_1 + E_2 < E_1 + E_2$. This proves the **Theorem 1**.

Since the Hamitonian is uniquely determined except for a constant by the ground state density, the wavefunction of any state can be obtained by solving the Schrödinger equation with this Hamiltonian. In principle, all properties of the system are completely determined by ground state electron density.

Theorem 2 Since the wavefunction is a functional of $n(\vec{r})$ (by theorem1), so is evidently the kinetic and interaction energy. Therefore, we can define a universal energy functional $E[n]$, valid for any number of electrons and any external potential V_{ext}. And the ground state energy of system is the global minimum value of this functional, and the density $n(\vec{r})$ that minimizes the functional is the ground state density.

Proof From **Theorem 1**, all properties such as the kinetic energy, potential energy, etc., are uniquely determined if $n(\vec{r})$ is specified, then each properties can be considered as functional of $n(\vec{r})$, including the total energy of system of course,

$$E_{HK}[n] = T[n] + E_{int}[n] + \int d\vec{r}V_{ext}(\vec{r})n(\vec{r}) + E_{II} \tag{2.5}$$

$$= F_{HK} + \int d\vec{r}V_{ext}(\vec{r})n(\vec{r}) + E_{II}, \tag{2.6}$$

where E_{II} is the interaction energy of the nuclei. The functional $F_{HK}[n]$ de-

fined in eq includes all internal energy, kinetic and potential energy of the interacting electron system,

$$F_{HK} = T[n] + E_{int}[n], \tag{2.7}$$

which must be universal by construction since the kinetic and interaction energy of particles are functionals of the density. Now, consider a system with the ground state density $n_1(\vec{r})$ corresponding to external potential $V_{ext}(\vec{r})$. Following the two theorem above, the HK functional is equal to the expectation value of the Hamiltonian in the unique ground state, which has wavefunction ψ_1,

$$E_1 = E_{HK}[n_1] = \langle \psi_1 \mid H_1 \mid \psi_1 \rangle \tag{2.8}$$

Now, also consider a different density $n_1(\vec{r})$, which necessarily corresponds to a different wavefunction ψ_2. It follows that the energy E_2 of this state is greater than E_1, since

$$E_1 = \langle \psi_1 \mid H_1 \mid \psi_1 \rangle < \langle \psi_2 \mid H_1 \mid \psi_2 \rangle = E_2. \tag{2.9}$$

Thus the energy given by Eq in terms of the HK functional evaluated for the correct ground state density $n_0(\vec{r})$ is indeed lower than the value of this expression for any other density $n(\vec{r})$. It follows that if the functional $F_{HK}[n]$ was known, then by minimizing total energy of the system with respect to variation in the density function $n(\vec{r})$, one could find the exact ground state densyt and energy.

2.1.2 Kohn-Sham formulation

Although HK provide the mathematical foundation of using electron density as a basic variable and ensure the existence of energy functional, but don't provide the exact form of energy functional for a given external potential. Without knowledge of energy functional, HK theorem is nothing but a change of problem from wavefunction to electron density.

One year after HK's publication, Kohn and Sham (KS) suggested a ingenious way of finding total energy functional, so called by KS ansatz [9]. The KS approach is to map the difficult interacting system to a noninteracting auxiliary system that can be solved much easily.

Before going further, consider the variational problem presented in the 2nd HK theorem and the point where difficulties arise. The ground state energy of a many electron system can be obtained by minimizing the total energy functional, subjected to the constraint that the number of electron is fixed to N, which leads to

$$\delta\Big[F_{HK}[n] + \int d\vec{r} V_{ext}(\vec{r}) n(\vec{r}) - \mu\Big(\int d\vec{r} n(\vec{r}) - N\Big)\Big] \tag{2.10}$$

and the corresponding Euler-Lagrange equation is given by

$$\mu = \frac{\delta F_{HK}[n(\vec{r})]}{\delta n(\vec{r})} + V_{ext}(\vec{r}) \tag{2.11}$$

where μ is the Lagrange multiplier associated with constraint.

The idea of KS is to set up a system where the kinetic energy could be determined exactly, since this is a main source of error in TF theory which

is unable to sustain the bound state. This was achieved by invoking a noninteracting system of electrons. The corresponding ground state wavefunction psi ks for this system is given by a single Slater determinant. The universal energy functional FHK is then partitioned in to three parts, noninteracting kinetic energy T_s, Hartree energy E_H and exchange-correlation energy E_{xc}. The first two of which can be calculated and constitute the majority of total energy. The third term includes all quantum mechanical and many-body interacting effect of correlation. Though all the difficulties of many-body problem are grouped into this third therm, the portion of this energy is small compared with first two term and dividing total energy into those three terms is the ingenuity of KS approach.

In the KS description, the Euler-Lagrange equation of Eq becomes,

$$\mu = \frac{\delta T_s[n(\vec{r})]}{\delta n(\vec{r})} + V_{KS}(\vec{r}) \tag{2.12}$$

where the KS potential V_{KS} is then given by

$$V_{KS}(\vec{r}) = V_{ext}(\vec{r}) + V_H(\vec{r}) + V_{xc}(\vec{r}), \tag{2.13}$$

with the Hartree potential,

$$V_H(\vec{r}) = \int d\vec{r'} \frac{n(\vec{r'})}{|\vec{r'} - \vec{r}|} \tag{2.14}$$

and the exchange-correlation potential,

$$V_{xc}(\vec{r}) = \frac{\delta E_{xc}[n(\vec{r})]}{\delta n(\vec{r})}. \tag{2.15}$$

The crucial point to understand in KS theory is that the density obtained when solving the alternative noninteracting KS system is the same as the exact ground state density. The ground density is obtained by solving the one particle Schrödinger-like equation,

$$-\frac{1}{2}\nabla^2\psi_i(\vec{r}) + V_{KS}(\vec{r})\psi_i(\vec{r}) = \varepsilon_i\psi_i, \tag{2.16}$$

and the density is constructed from

$$n(\vec{r}) = \sum_{i=1}^{N} |\psi_i(\vec{r})|^2. \tag{2.17}$$

The non-interacting kientic energy T_s is therefore given by

$$T_s[n(\vec{r})] = -\frac{1}{2}\sum_{i=1}^{N}\int d\vec{r}\psi_i^*(\vec{r})\nabla^2\psi_i(\vec{r}). \tag{2.18}$$

2.1.3 Approximation of exchange-correlation energy : LDA and GGA

Although exact in principle, KS equation is approximate in practice because of the unknown exchange-correlation (XC) functional $E_{xc}[n]$. In the original paper of KS, they suggested an approximation for exchange-correlation functional, in which the exchange and correlation energy is simply an integral over space of exchange-correlation energy of locally homogenous electron gas with density assumed to be that of the considering system at that point. In other word, they considered an inhomogeneous electron gas system as a locally homogeneous electron gas system. This ap-

proximation is called local density approximation (LDA). This means that we can write the exchange-correlation energy as

$$E_{xc}^{LDA} = \int d\vec{r}\varepsilon_{xc}^{LDA}(n(\vec{r})), \tag{2.19}$$

where $\varepsilon_{xc}^{LDA}(n(\vec{r}))$ is the XC energy of homogeneous electron gas of density $n(\vec{r})$ per density and can be split into exchange and correlation contributions,

$$\varepsilon_{xc}^{LDA}(n(\vec{r})) = \varepsilon_{x}^{LDA}(n(\vec{r})) + \varepsilon_{c}^{LDA}(n(\vec{r})) \tag{2.20}$$

The exchange energy of homogeneous electron gas is exactly given by Dirac's solution,

$$\varepsilon_{x}^{LDA}(n(\vec{r})) = -\frac{3}{4}\left(\frac{3}{\pi}\right)^{\frac{1}{4}} n(\vec{r})^{\frac{1}{3}} = -\frac{3}{4}\left(\frac{9}{4\pi^2}\right)^{\frac{1}{4}} \frac{1}{r_s}, \tag{2.21}$$

where r_x is the average distance between electrons.

The correlation energy parameter by Perdew and Zunger based on the quantum Monte Carlo simulation of Ceperley and Alder.

In the real system, electron density is far from homogeneous electron gas and it may at first seem somewhat surprising that such crude approximation for inhomogeneous electron gas system is so successful. This can be partially explained with the concept of XC hole which is defined as

$$n_{xc}(\vec{r},\vec{r'}) = n(\vec{r'}[g(\vec{r},\vec{r'}) - 1]) \tag{2.22}$$

$$g(\vec{r},\vec{r'}) = 1 - \frac{|n_{xc}(\vec{r},\vec{r'})|^2}{n(\vec{r})n(\vec{r'})} \tag{2.23}$$

The XC hole nxc represents a fictious charge depletion due to exchange and correlation effect, i.e., due to the fact that presence of an electron at r reduces the probability of finding a second electron at $\vec{r'}$ in the vicinity of $\vec{r}$. The success of LDA comes from the short-ranged nature of n_{xc} in the real system and the correct sum rule inscribed in this approximation [10].

A natural extension of LDA to improve the accuracy is to include the higher order terms, gradient and higher order derivatives of density to take into account the inhomogeneity of the electron density. The approximation to include the magnitude of gradient of density eq is named as gradient expansion approximation (GEA). However, GEA does not lead to the desired accuracy, but frequently leads to even worse results than LDA due to the violation of the sum rule and other relevant conditions. For this reason, generalized gradient approximation (GGA) is proposed to improve calculation accuracy by preserving desired properties of exact sum rule. Among various GGA, GGA by Perdew, Burke and Ernzerhof (PBE) [11] is the most popular one, because it satisfies many exact conditions for the XC hole and contains only single fitting parameter which is not sensitive to the accuracy of result. The detailed form of PBE GGA is given in the following. The correlation is

$$E_c^{PBE}[n^{\uparrow}, n^{\downarrow}] = \int d\vec{r}[\varepsilon_c^{hom}(r_s, \zeta) + H(r_s, \zeta, t)] \tag{2.24}$$

where,r_s and ζ are the mean electron-electron distance and magnetization density. $E_c^{hom}(r_s, \zeta)$ is the correlation energy of homogeneous electron gas. $t = \frac{|\nabla|}{2\phi k_s n}$ is a dimensionless density gradient with $\phi = [(1+\zeta)^{2/3} + (1-\zeta)^{2/3}]/2$ and $k_s = \sqrt{4k_F/\pi a_0}$ is the TF screening wavenumber. THe function

H is,

$$H = \frac{e^2}{a_0}\gamma\phi^3 \log\Big[1+\frac{\beta}{\gamma}t^2\Big(\frac{1+At^2}{1+At^2+A^2t^4}\Big)\Big], \tag{2.25}$$

where,

$$A = \frac{\beta}{\gamma}\Big[exp\Big(\frac{-\varepsilon_c^{hom}}{\gamma\phi^3 e^2/a_0}\Big)-1\Big]^{-1} \tag{2.26}$$

The exchange term of PBE GGA is

$$E_{PBE}x[n^{\uparrow},n^{\downarrow}] = \int d\vec{r}\varepsilon_x^{hom}(n(\vec{r}))F_x(s), \tag{2.27}$$

where ε_x^{hom} is the exchange energy density of homogeneous electron gas. The enhancement factor is

$$F_x(s) = 1+\kappa-\frac{\kappa}{1+\mu s^2/\kappa} \tag{2.28}$$

where, $\kappa = 0.804, \mu = 0.21951$ and $s = |\nabla n|/2k_F n$.

2.2 Pseudopotential Planewave method

2.2.1 Planewave basis set

To solve the Schrödinger equation or one particle KS equation numerically, we should introduce the appropriate basis set to present wavefunctoin. There are many choices such as numerically constructed orbitals, Gaussian orbitals, planewaves, augmented planewaves and real space grids. Among them, we will briefly survey on the planewaves and real grid basis set. Planewaves are solutions of the Schrödinger equation in the uniform

external potential, as is approximated verified in the interstitial regions in condensed phase. In general external potentials, the wavefunctoin can be always written as a linear combination of planewaves.

Unlike other orbital-based basis, the planewave basis set is a floating basis set, in other words, it does not depend on the position of nuclei in a matter. This property is practically very important. They represent all regions of space with same accuracy and there are no additional forces on the nuclei arising from the derivation of the basis function. This is because the Hellman-Feynman Theorem [12] can be strictly applied only when the basis set is fully converged, or when the basis functions do not depend on the nuclei positions. Another advantage is that the kinetic energy term in one electron Hamiltonian is diagonal in reciprocal space, while the potential term is local in space. This feature can be exploited to speed up the calculations by transforming the wavefunctoin and the density back and forth from real to reciprocal space and vice versa. The transformation can be done very efficiently by using fast Fourier transformation (FFT), whose associated computational cost scales NlogN, where N is the number of planewaves.

On the other hand, the one of the main disadvantage is that systems where the wavefunction varies rapidly close to the nuclei require a very large number of planewaves. The bare Coulomb potential is far from constant external potential so that the naïve approach to represent the true wavefunction proves to be too demanding. This is the motivation for the development of pseudopotential theory.

2.2.2 Pseudopotential approximation

The fundamental idea of pseudopotential approximation is the replacement of the strong core potential with another softer potentials. The scattering properties of a localized spherical potential at any energy can be formulated concisely in terms of the phase shift, which determines the cross-section and all properties of the wavefunction outside the localized region. The goal of pseudopotential is to replace one potential with a different soft potential with the same phase shift module 2π. The general form of pseudopotential is

$$V_{PS} = \frac{Z_i on}{r} + \sum_c (\varepsilon_v - \varepsilon_c) \mid \phi_c \rangle \langle \phi_c \mid, \tag{2.29}$$

where Z_{ion}/r is the bare nuclear potential, $\mid \phi_{c(v)} \rangle$is the core (valence) state, and $\varepsilon_{c(v)}$ is the core (valence) energy eigenvalues. The pseudo wavefunctions are written as

$$\mid \phi_v^{PS} \rangle = \mid \phi_v \rangle + \sum_c a_{vc} \mid \phi_c \rangle \tag{2.30}$$

with $a_{vc} = \langle \phi_C \mid \phi_v^{PS} \rangle$.

It is easily verified that the above pseudopotential has the same eigenvalue with the original potential, but with different (pseudo) wavefunctions. It is noted that the non-uniqueness of pseudopotential allows the freedom to choose forms that simplify the calculations and the interpretation of the resulting wavefunction.

Desirable properties of pseudopotential are that the potential should be

as soft as possible and transferable. The transferability means that the constructed pseudopotential in one reference circumstance (chemical environment) should well reproduces the original potential in other circumstance. For example, a carbon pseudopotential which reproduces true carbon atom's eigenvalues should also produce diamond's and graphite's electronic and mechanical properties. Hamann, Schluter, and Chang (HSC) [13] found that the transferability is guaranteed by imposing the following condition.

$$\int_0^{r_c} dr r^2 \mid \phi^{PS}(r) \mid^2 = \int_0^{r_c} dr r^2 \mid \phi^{AE}(r) \mid^2 \tag{2.31}$$

where r_c is a cutoff radius. This is called norm-conserving condition. A key result of HSC was to realize that the norm of the wavefunction also appears in a very important identity related to the Friedel sum rule,

$$-\frac{1}{2}\left[[r\phi(\varepsilon,r)]^2 \frac{d}{d\varepsilon}\frac{d}{dr}\log\phi(\varepsilon,r)\right]_{r_c} = \int_0^{r_c} dr r^2 \mid \phi(r) \mid^2 . \tag{2.32}$$

Therefore, the norm-conserving condition imposes that to first order in the eigenvalue, the true and pseudo wavefunction vary in the same way. This implies that a small change in the eigenvalue due to changes in the external potential produces only a second order change in the logarithmic derivatives. One should be keep in mind the pseudopotential is useful, not in every energy range, but at least in environment such that the eigenvalues do not depart significantly from the eigenvalues used in its construction. It is clear from eq that a pseudopotential acts differently on wavefunctions of

different angular momenta. This type of pseudopotential is called semi-local form and can be written as

$$\hat{V}_{PS}(r) = \sum_{l=0}^{\infty} \sum_{m=-l}^{l} v_{PS}^{l}(r) \mid lm\rangle\langle lm \mid = \sum_{l=0}^{\infty} v_{PS}^{l}(r)\hat{P}_l \tag{2.33}$$

where v_{PS}^{l} is the pseudopotential corresponding to angular momentum l, and the operatior $\hat{P}_l = \sum_{m=-l}^{l} \mid lm\rangle\langle lm \mid$ is a projection operator onto the l-th angular momentum. This semi-local term can be recast as a sum of local and non-local terms as following,

$$\hat{V}_{PS}(r) = V^{local}(r) + \sum_{l=0}^{\infty} \delta v_{PS}^{l}(r)\hat{P}_l \tag{2.34}$$

The non-local term can be replace, to a good approximation, by a separable operator eq which is fully non-local in both l and m, and radius r so that we obtain the Kleinman-Bylander (KB) separable form [14]

$$\hat{V}_{KB}(r) = V^{local}(r) + \sum_{lm} \frac{\mid \phi_{lm}^{PS}\delta v_{PS}^{l}\rangle\langle\delta v_{PS}^{l}\phi_{lm}^{PS} \mid}{\langle\phi_{lm}^{PS} \mid \delta v_{PS}^{l} \mid \phi_{lm}^{PS}\rangle} \tag{2.35}$$

The softness and transferability are also greatly improved by Vanderbilt's ultrasoft pseudopotential [15]. He removed the norm-conserving condition which limits the softening pseudization of nodeless wavefunctions such as carbon or oxygen p-orbital by replacing the original eigenvalue problem with a generalized eigenvalue problem. Furthermore, with multiple projectors in a separable form, the energy range incorporated in the construction can be arbitrarily increased. The recent progress of pseudopotential allows the recovery of core region. In the projector augmented wave

(PAW) method by Blochl and Kless and Joubert [16, 17], the true and psedo wavefunction are related by a linear transformation, which is assumed to be unity except for a sphere centered on the nuclei. The transformation operator can be written as

$$T = 1 + \sum_m (\mid \phi_m^{AE}\rangle - \mid \phi_m^{PS}\rangle)\langle \bar{p}_m \mid, \tag{2.36}$$

where ϕ_m^{AE} are all-electron partial waves centered on nuclei, ϕ_m^{AE} are pseudo atomic partial waves that coincide with the all-electron one outside a cutoff radius and match continuously inside and $\bar{p}_m$ are projectors that verify the duality relation

$$\langle \bar{p}_m \mid \phi_n^{AE}\rangle = \delta_{mn}. \tag{2.37}$$

For any operator $\hat{A}$ in the original all-electron problem, we can introduce a transformation operator T operating on the smooth part of the wavefunction

$$\tilde{A} = \hat{A} + \sum_{mm'} \mid \bar{p}_m\rangle \left[\langle \phi_m^{AE} \mid \hat{A} \mid \phi_{m'}^{AE}\rangle - \langle \phi_m^{PS} \mid \hat{A} \mid \phi_{m'}^{PS}\rangle\right] \langle \bar{p}_{m'} \mid . \tag{2.38}$$

The PAW method is what we used in the first-principles calculation and is implemented in ab initio package VASP

2.3 Molecular Dyanmics Simulation

Molecular dynamics (MD) simulation is a computational method which connects principle to phenomena. In the classical particle approximation, the trajectories of atoms and molecules are completely determined by Newton's equation of motion and all every physical quantities can be calculated with the knowledge of forces between particles. Therefore, solving differential equation analytically or numerically is the central issue for the understanding multi-particle systems.

In a computational sense, MD simulation is a numerical integration of coupled 2nd order differential equation. At every time step, forces acting on the particles are calculated using force field and the position and velocity of particles are updated according to Newton's equation of motion. Therefore, accurate and transferable force field and position-momentum integration methods are essential element for successful simulation. The oldest, most popular but efficient integrator is Verlet algorithm. For a 2nd order differential equation of type eq with suitable initial conditions for initial value and its 1st derivative, the update of function in the Verlet algorithm is summarized as follows,

$$\vec{x}_1 = \vec{x}_0 + \vec{v}_0 \Delta t + \frac{1}{2} A(\vec{x}_0) \Delta t^2, \tag{2.39}$$

$$\vec{x}_{n+1} = 2\vec{x}_n - \vec{x}_{n-1} + A(\vec{x}_0) \Delta t, \; for \; n \geq 2 \tag{2.40}$$

The Verlet algorithm uses the position and accelerations at time t, and

the position from the previous step, to calculate the updated position at t+ dt. The velocities do not explicitly appear in the formula.

The dynamical system under the conservative potential conserve total energy and the phase space trajectory of system always lies on the states of a microcanonical ensemble. In the real situations, however, system under the consideration interacts environment. In the equilibrium, total dynamical energy of system fluctuates around mean average value, which is determined by canonical ensemble with given temperature. From the early ages of MD simulations, there are many attempts to introduce temperature and random fluctuation effects to deterministic and energy conserved MD simulation. Among many constant-temperature MD simulation techniques, the algorithm originally developed by Nose and further improved by Hoover [18, 19] is the most elegant and commonly used one. In the approach of Nose, a Hamiltonian with an extra fictitious degree of freedom for heat bath is introduced as follows,

$$H(\vec{P},\vec{R},p_s,s) = \sum_i \frac{\vec{p}_i^2}{2ms^2} + \frac{1}{2}\sum_{i,j} U(\vec{r}_i - \vec{r}_j) + \frac{p_s^2}{2Q} + gk_BT\log(s) \quad (2.41)$$

where g is the number of momentum degrees of freedom and Q is an imaginary mass which controls temperature fluctuation of the system. $\vec{P}$ and $\vec{R}$ represent all coordinates. Time evolution of total dynamical system, system plus single fictitious degree of freedom, under the extended Hamiltonian is limited on the constant energy surface in the phase space (microcanonical ensemble), but it is easy to show that phase space density projection on the

real system's degrees of freedom is given by Boltzmann weight.

2.4 Monte Carlo Method

Many physical quantities in statistical mechanics are obtained by integrating many coupled degrees of freedom. For example, calculation of average kinetic energy of system composed of N-particle requires 6N-dimensional phase space integration and average magnetic moment of N Ising spin system requires summation of 2N possible configurations. It can be easily seen that computational cost of integration (or summation) increases exponentially with the number of degrees of freedom and exceeds computational power of modern computer.

Basically, the Monte Carlo (MC) method is developed to overcome above computational difficulties on multi-dimensional integration. In this method, integrating all possible configurations is approximated by summation of small number of certain configurations of a desired (or pre-defined) probability distribution, i.e.,

$$\langle A \rangle = \int A(\vec{r},\vec{p}) e^{-\beta E(\vec{r},\vec{p})} d\vec{r} d\vec{p} / Z \approx \frac{1}{N} \sum_{i=1}^{N} A(\vec{r}_i,\vec{p}_i) e^{-\beta E(\vec{r}_i,\vec{p}_i)} d\vec{r} d\vec{p} / Z \tag{2.42}$$

Therefore, obtaining a good sample configuration is a key element for the successful realization of MC methods and many sampling algorithms are proposed for different usage. In the statistical physics, the Metropolis-Hastings Algorithm (MHA) is the most popular algorithm for obtaining a

sequence (or a set) of configurations. Below is a flow chart of MHA for finding a single sequence of configuration g_n.

1. Initialize an input image g_1

2. Repeat

2.1 Generate image g_2 by performing a random trial move from g_1

2.2 Compute transition probability $T(g_1, g_2) = min[1, P(g_2)/P(g_1)]$, where $P(g)$ is the probability of g

2.3 if a random number in (0,1) $< T(g_1, g_2)$ then $g_2 \rightarrow g_2$ else $g_1 \rightarrow g_2$ (not updated)

3. Until equilibrium is attained.

In the canonical ensemble, probability function $P(g)$ is simply given by Boltzmann factor of image g, i.e., $P(g) = e^{\frac{-E(g)}{k_B T}}$.

Different initial configuration g_1 bears different final (or equilibrium) configuration g_{eq}. If we repeat those process with different initial configuration g_1, the set of g_{eq} is a good sample configuration for the approximate integration in equation.

Chapter 3

Hydrogen Storage in Potential Well Using Potassium-Intercalated Graphite Oxide

Using *ab intio* electronic structure calculations and grand canonical Monte Carlo simulations, we investigate the storage capacity of hydrogen molecules in potassium intercalated graphite oxide. We show that the binding energy of hydrogen between layers of graphene oxide is mainly originated from the dispersion interaction and further increased by induced dipole interactions. Its strength is fairly insensitive to the position of the hydrogen molecule on the graphene plane and the storage capacity is enhanced basically by the corresponding Boltzmann factor. The trend of storage capacity with different geometries and chemical compositions of scaffold materials is explained. We also examine the effect of the potassium ion clustering on the storage capacity.

3.1 Introduction

Hydrogen has been considered to be a clean and sustainable future energy source [1], but storing hydrogen safely and efficiently at ambient conditions is a major obstacle in commercializing hydrogen fuel-cell pow-

ered vehicles. Metal or chemical hydrides show high storage capacity [2] but do not satisfy the requirements for the fast kinetics and reversibility. Metal-organic frameworks (MOFs) have been regarded as promising storage materials owing to its porosity, fast kinetics, and the reversibility [3, 4], but high pressure and cryogenics are necessary in the adsorption process because of the weak adsorption energy of hydrogen molecules mainly via van der Waals interactions ($\approx$0.05eV/H_2). It has been found that the optimal binding energy for the ambient condition storage ($\approx$0.3eV/H_2) is realizable by introducing transition-metal (TM) atoms into MOFs [5, 6]. TM atoms are bound to the linker part of MOFs and H_2 molecules are adsorbed to the TM atoms through the so-called Kubas interaction [7]. However, because of high cohesive energy and reactivity, TM atoms tend to form clusters and are easily contaminated by other gas molecules, thereby hindering the experimental realization of the goal of the storage density set by the DOE by the year of 2020 (5.5wt% and 40g/L).

Recently, it has been shown that a class of materials based on pillared graphene layers have large surface areas and the magnitude of the hydrogen binding energy with the material increases to 0.15eV/H_2 by functionalization and alkali metal ion doping[20, 21, 22]. This binding energy is not strong enough to adsorb H_2 at the binding sites at room temperature, but the large surface area and the void space make it possible to store hydrogen in the gas form. For example, Deng *et al*. proposed alkali-doped pillared carbon materials to maximize reversible H_2 storage and suggested a possible scheme to synthesize practical storage materials[20]. Dimitrakakis *et al*. used lithium-doped 3-dimensional carbon nanostructures as a stor-

age material and showed that the induced dipole interaction between H_2 and doped lithium increases volumetric storage capacity up to 41g/L under ambient conditions[21]. Tylianakis *et al.* studied hydrogen storage capacity of lithium-doped graphite oxide, and explained that storage capacity is closely related to the pore volume and the carbon to oxygen ratio of graphite oxide[22].

In this study, we propose a storage mechanism based on the diffusive equilibrium between systems with different potentials and also suggest a storage material for the realization of this mechanism. The equilibrium condition of hydrogen inside and outside the material is $\mu_{in} = \mu_{out}$, where μ is the chemical potential of the hydrogen molecule. If the material provides, as afirst-order approximations, a uniform potential well with the depth of V (< 0) relative to outside, we will show later that gas density in the potential well is $e^{-\frac{V}{k_B T}}$ times larger than that outside the potential[23], T is the temperature and k_B is the Boltzmann constant. The exponential dependence of the density inside the material on V allows for the practical room temperature storage with a relatively small potential depth (the enhancement factor $e^{-\frac{V}{k_B T}}$ turns out to be 100 for V =-0.12eV at 25°C). Since an experimental technique of tailoring a strict 3-dimentional (3D) attractive potential for a nonpolar molecule is not available in practice, we have searched for 2-dimentional (2D) materials that interact with hydrogen molecules with desired binding strength. For example, if the interlayer distance **d** (in the z-direction) of graphite is increased to twice the equilibrium distance between a H_2 molecule and a single-layer graphene, then H_2 can penetrate in between the layers and it interacts with both upper and lower layers. In this

situation, the van der Waals (dispersion) interaction energy between H_2 and two graphene layers may reach ≈-0.10eV and an extra binding energy of only a few tens of meV is enough for practical room temperature storage. Furthermore, the van der Waals interaction is almost independent of the xy position of so H_2 that H_2 molecules behave almost like a gas in 2D as desired [24, 25].

As a realization of the layered structure of enhanced **d** derived from graphite, we suggest a potassium intercalated graphite oxide (KGO) as a possible storage material. In recent experiments, it was reported that **d** of graphite can be increased to 6-7 Å by oxidation and further increased to 1nm or more by potassium intercalation [26]. In the experiment, the graphite oxide (GO) was dispersed in the KOH aqueous solution to expand the layers and was hydrothermalized to remove moistures [27]. Although the proposed storage material here (KGO) is somewhat similar to other porous materials, the storage mechanism is much different. In our storage mechanism, the H_2 molecules vigorously move around inside the potential well originated mainly from the H_2-graphene layer interaction. This is clearly distinct from the H_2 storage mechanism of aforementioned study, where a hydrogen molecule binds at a particular binding site and the storage material (whether it is a MOF, any carbon-based material, or others) is used to provide the scaffold structure to maintain binding sites. In the material we propose, on the other hand, a more or less uniform potential in the void space is desirable to achieve a gas-phase storage in the potential well.

3.2 Methods

We performed *ab inito* density functional theory (DFT) electronic structure and total energy calculations [8, 9] and obtained the H_2 potential energy surface (PES) of the system. In the calculation, a generalized gradient approximation of Perdew *et al.* [11] with the Grimme-type [28] van der Waals interaction correction was employed to describe the exchange-correlation energy in the Vienna ab initio simulation package (VASP) [17]. The energy cutoff of 400eV was used for the projector-augmented wave pseudopotential basis set. In the atomic structure relaxation, the atomic configuration was adjusted until the Hellmann-Feynman force on each atom was less than 0.01eV/Å. To quantify the storage capacity of materials at finite temperature, we performed grand canonical Monte Carlo (GCMC) simulations. In the CGMC simulations, a hydrogen molecule was modeled as a single classical point particle and the intermolecular (H_2-H_2) interaction was described by the Silvera-Goldman potential [29].

3.3 Results and discussion

Local atomic configurations and the chemical composition of KGO depend stongly on synthesis conditions[30] and their precise determination in experiment is still difficult. On the theoretical side, there were efforts to search for structure of GO with various functional group coverage [31, 32], but only a small set of configurations were examined in most cases due to computational limitations. After the calculation of atomic relaxations, we found that all oxygen atoms were strongly bound to carbon atoms

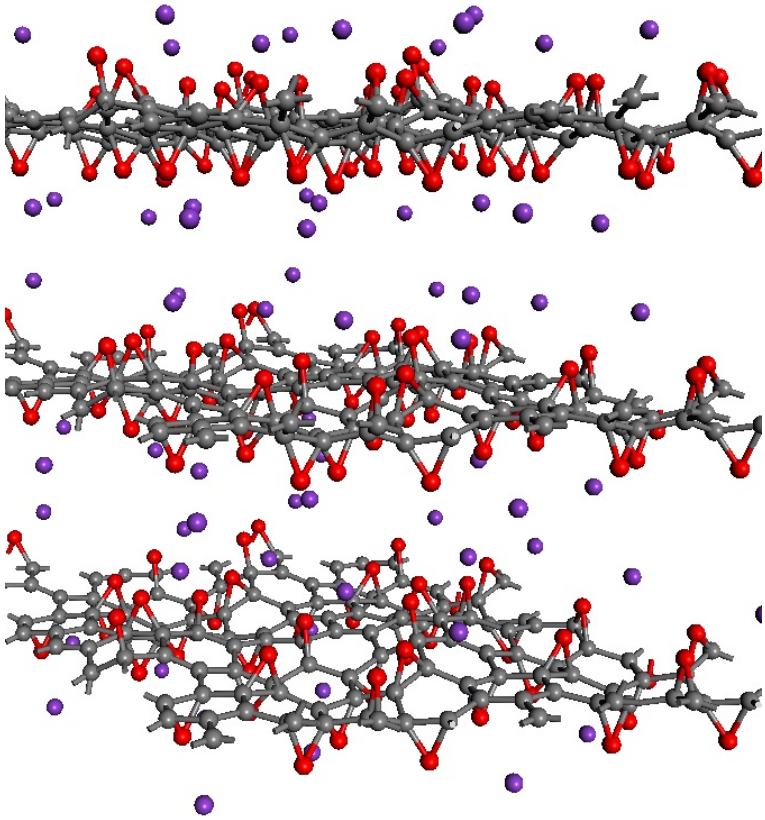

Figure 1: Model atomic structure of KGO. Gray, red and purple dots represent carbon, oxygen and potassium atoms, respectively.

and formed epoxy groups. Potassium atoms were attached near the oxygen atoms (Figure 1). For computational simplicity, pillar molecules between layers (which should exist in reality to maintain the interlayer distance **d**) were ignored and **d** was kept constant in the relaxation calculation.

The interaction between a hydrogen molecule and KGO used in the GCMC simulation is assumed to be the sum of the potentials contributed from each constituent of KGO, i.e., graphene layer, epoxy or pottasium-

attached epoxgy group (K-epoxy),

$$\begin{aligned} V_{H_2-KGO}(\vec{r}) =& V_{H_2-graphene}(\vec{r}) + \sum_i V_{H_2-epoxy}(\vec{r}-\vec{r}_{epoxy,i}) \\ &+ \sum_i V_{H_2-K-epoxy}(\vec{r}-\vec{r}_{K-epoxy,i}) \end{aligned} \tag{3.1}$$

where, $V_{H_2-graphene}(\vec{r})$ is the interaction potential between H_2 and graphene layers and $V_{H_2-A}(\vec{r}-\vec{r}_{A,i})$ is interaction potential between H_2 and the i^{th} functional group of type A (A = epoxy or K-epoxy) at position $\vec{r}_{A,i}$.

We define the potential energy of a H_2 molecule as a function of its position in the space between layers as follows,

$$V(\vec{r}) = E[M + H_2(\vec{r})] - E[M] - E[H_2] \tag{3.2}$$

where M is the storage material (KGO) interacting with H_2 and $E[S]$ is the total energy of the isolated system S.

Figure 2 shows the PES of a single K-epoxy on the 4×4 graphene supercell in the plane parallel (x-y plane) to the graphene layer at z=3Å. In the calculation, the x-y plane is partitioned into 30×30 grids parallel to the lattice vector of a unit supercell and the energy optimization is done with the constraint of the center of the H_2 molecule kept fixed at each grid point. The PES of arbitrary points is obtained by the spline interpolation. The average potential energy of the accessible region (where V<0) at the plane 3Å above the graphene layer is -83meV, which is 23meV stronger than that of pristine graphene layer of -60meV (via van der Waals interaction only). The deepest potential near the potassium ion reaches -0.16eV. The enhance-

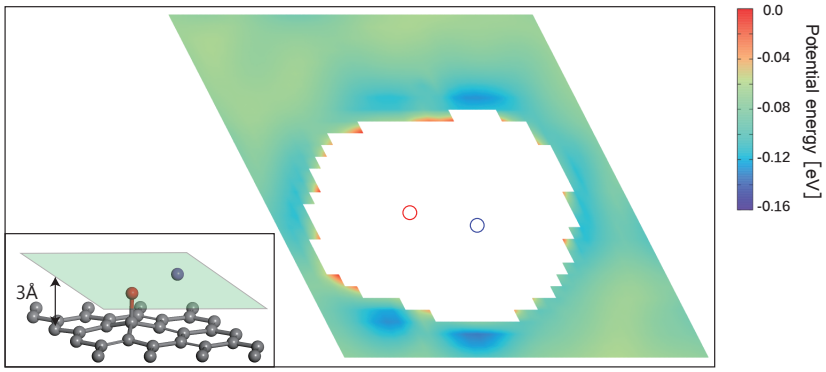

Figure 2: Potential energy surface of a H_2 molecule on the 4×4 graphene supercell with a potassium-attached epoxy group. The plane of the plot is parallel with and 3Å above the graphene layer (green parallelogram in the inset). The region of the positive potential energy is drawn in white color. Positions of the oxygen and potassium atom are denoted by red and blue circles, respetively. The inset shows the atomic configuration of the unit supercell in the *ab initio* calculation.

ment of the attractive potential by functionalization is attributed to induced dipole interactions of H_2 with the electric field generated by oxygen atoms or potassium ions (and a minute orbital hybridization) [33, 22]. According to atomic charge analysis [34], an potassium atom donates nearly one electron to graphene and the epoxy group, and becomes a positive ion (K+). The magnitude of the electric field at the position of the largest potential is 1.78V/Å, and we can estimate roughly the contribution of the induced dipole interaction to binding energy ($E_{ind} = -\frac{1}{2}\alpha \mid \vec{E} \mid^2$, α is the polarizability of H_2 molecule) is -0.11eV. The region of the positive potential energy (V>0) close to the oxygen and potassium atom due to the steric hindrance (thus inaccessible to the H_2 molecule) is represented in white color.

GCMC simulation results of the gravimetric and volumetric storage ca-

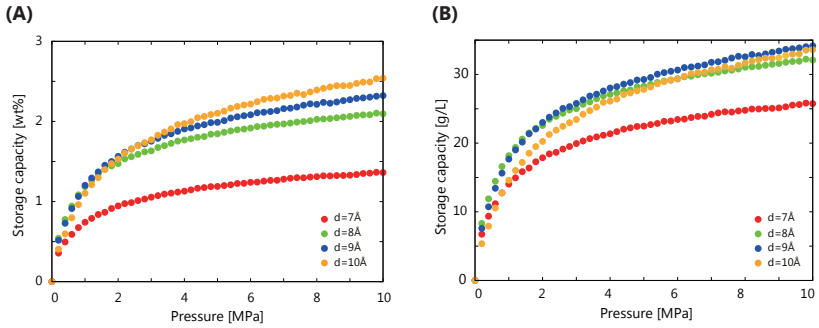

Figure 3: Room temperature (A) gravimetric and (B) volumetric storage capacity of KGO $CO_{0.25}K_{0.125}$ with different **d**.

pacity as a function of pressure P $\leq$ 10MPa at 300K of KGO with different **d**'s are shown in Figure 3. Lennard-Jones parameters of H_2-exopy/K-epoxy and H_2-carbon necessary for the simulation were extracted from the calculated PES (Table 1). The trend of storage capacity can be explained in terms of the density enhancement factor and the accessible volume V_{acc} (withe the negative potential energy) inside the KGO layers. The interaction between hydrogen and KGO gives rise to the formation of the relatively uniform attractive potential well between the KGO layers, and the equilibrium hydrogen density inside the KGO, n_{in}, is much higher than that of outside the KGO (the H_2 reservoir), n_{out}. For an ideal gas, the local equilibrium density

Table 1: Parameters of the Lennard-Jones interaction potential ε_{H_2-A}, σ_{H_2-A}, and the interaction cutoff $r_{H_2-A}^{cutoff}$ for A = epoxy, K-epoxy, and carbon

A	ε_{H_2-A} [meV]	σ_{H_2-A} [Å]	$r_{H_2-A}^{cutoff}$ [Å]
Carbon	5.4	2.97	6.0
Epoxy	11.0	2.70	7.0
K-Epoxy	60.0	2.50	7.0

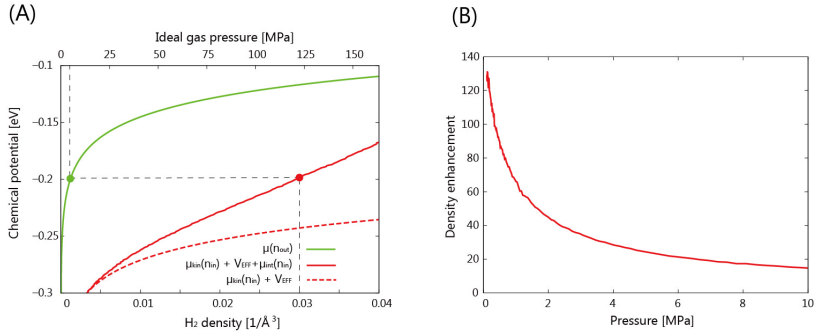

Figure 4: (A) Chemical potential as a function of the H_2 density (lower x-axis) outside (green curve, RHS of Eq. 3.3) and inside (solid red curve, LHS of Eq. 3.3) the KGO ($CO_{0.25}K_{0.125}$ with **d**=10Å) . For comparision, the dashed red curve represents the chemical potential inside the KGO layer under the ideal gas assumption. The upper x-axis is the ideal gas pressure corresponding to the gas density in the lower x-axis. (B) Density enhancement factor X as a function of the H_2 pressure outside the KGO layer. $T = 300K$ in all cases.

enhancement at position $\vec{r}$ follows the Boltzmann factor, $n_{in}(\vec{r}) = n_{out}e^{-\frac{V(\vec{r})}{k_BT}}$ as mentioned before. The average density enhancement factor, $X = \frac{n_{in}}{n_{out}}$, is given by $\frac{1}{V_{acc}}\int_{V_{acc}} e^{\frac{-V(\vec{r})}{k_BT}}d\vec{r}$. In case of a uniform potential,$V(\vec{r}) = V_0$, and X is given by $e^{\frac{-V_0}{k_BT}}$ as stated in the Introduction. For a non-ideal gas, on the other hand, the contribution of intermolecular interactions to the chemical potential inside the material ($\mu_{int}(n_{in})$) is nonnegligible and should be taken into account to obtain the correct density enhancement. The n_{in} is determined by solving the chemical potential equality inside and outside the KGO,

$$\mu_{kin}(n_{in}) + V_{EFF} + \mu_{int}(n_{in}) = \mu(n_{out}). \tag{3.3}$$

Outside the storage material, the $H_2 - H_2$ interaction is sufficiently small

as long as we are interested in the pressure P $\leq$ 10MPa at room temperature. We make an ideal-gas approximation that $\mu(n_{out}) = -k_B T \log(n_{out}\lambda^3)$, where λ is the thermal wavelength ($=\frac{h}{\sqrt{2\pi m k_B T}}$, where h is the Planck constant and m is the mass of the H_2 molecule). The contribution to the μ from rotational and vibrational motion not included here will be discussed latter. In Eq.3.3, $V_{EFF} = -k_B T \log\left(\frac{1}{V_{acc}}\int_{V_{acc}} exp\left[-\frac{V(\vec{r})}{k_B T}\right] d^3\vec{r}\right)$ is the effective external potential, and $\mu_{int}(n) = -k_B T \log\left(\frac{1}{V_{acc}}\int_{V_{acc}} \langle exp\left[-\frac{V_{int}(\vec{r};\vec{r}^{N-1})}{k_B T}\right]\rangle_{N-1} d^3\vec{r}\right)$ is the chemical potential from intermolecular interaction [24, 35]. N is the number of particles in volume V_{acc} ($N = nV_{acc}$), $\langle ...\rangle_N$ denotes canonical ensemble average over the configuration space of the N-1 particle system and $V_{int}(\vec{r};\vec{r}^{N-1})$ is the interaction potential between a particle at $\vec{r}$ and other N-1 particles at $N-1$ particle configuration space $\vec{r}^{N-1}$. Figure 4 shows a graphical solution of Eq. 3.3 and the density enhancement as a function of the H_2 pressure in the ouside reservior. For example, if the H_2 pressure outside the KGO is 5MPa (green dot in the Figure 4(A)), the chemical potential is $\approx$-0.2eV. The corresponding H_2 density inside the KGO layer (solution of Eq. 3.3) is given by $\approx 0.03/\text{Å}^3$ (red dot in the Figure 4(A)) and the density enhancement factor X at the room temperature ($T = 300K$) is $\approx$24. Not all space inside the KGO layer is available for storage, because the strong repulsive interaction between a H_2 molecule and functional groups prohibits hydrogen molecule from approaching the region of the positive potential near the functional groups. Storage capacity is basically the product of three quantities : density in the outside KGO layer, the volume of the space of negative potential inside the KGO layer, and the density enhancement fac-

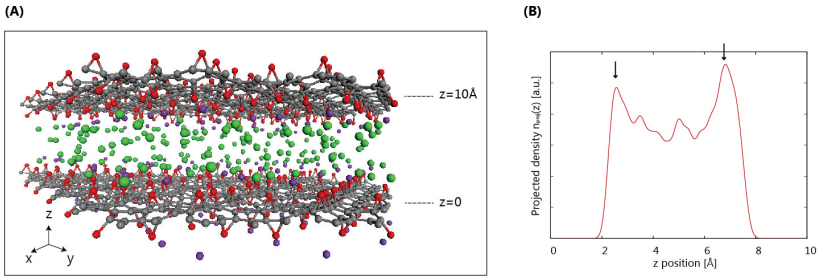

Figure 5: (A) Snapshot of the grand canonical Monte Carlo simulation after reaching the equilibrium. Gray, red, purple and green dots represent carbon, oxygen, potassium, and hydrogen molecules, respectively. (B) z-axis-projected density of hydrogen molecules, $n_{proj}(z) = \int_{xy} n(x,y,z)dxdy$, between two KGO layers located at $z = 0$ and $z = 10$ Å. Peak positions in the distribution of hydrogen molecules are indicated by arrows.

tor due to the negative potential, i.e., the storage capacity=$cn_{out}XV_{acc}$. The proportionality constant c is related with the mass (or volume) density of KGO.

At very low pressure ($\lesssim$ 0.5MPa), the hydrogen density both inside and outside the KGO are low so that the average intermolecular distance is larger than the H_2-H_2 interaction range. In this case, hydrogen molecules behave like an ideal gas and the contribution of intermolecular interaction to the chemical potential is very small. In Figure 4, the chemical potential difference between interacting gas (solid red curve) and ideal gas inside (dashed red curve) the KGO layer is very small (Figure 4 (A)), and the corresponding density enhancement factor is approximately given by $e^{-\frac{V_{EFF}}{k_BT}}$ (Figure 4 (B)). Thus storage capacity is linearly related with pressure, and its slope is proportional to $\frac{1}{k_BT}e^{-\frac{V_{EFF}}{k_BT}}V_{acc}$. The slope of for the KGO with **d**=8Å is the steepest among the four cases (**d**=7Å, 8Å, 9Å, and 10Å). This

indicates that of $|V_{EFF}|$ is the largest when **d**=8Å, because 8Å is about twice the equilibrium distance between the hydrogen molecule and a single layer of KGO; the hydrogen molecules interacts with both upper and lower layers. Although V_{acc} for **d**=8Å is less than that of **d**=9Å or **d**=10Å, the storage capacity depends linearly on V_{acc} but exponentially on V_{EFF}, so that increasing $|V_{EFF}|$ is more effcitve for low pressure sotrage.

At higher pressure, on the other hand, the contribution of the repulsive intermolecular interaction to the chemical potential is substantial. In this case, the total effective potential becomes less attractive the density enhancement factor gets smaller. Here, a larger V_{acc} becomes a more important factor than in the lower pressure case, and a larger **d** creates a larger V_{acc} inside the layers, leading to a higher storage capacity. A quasi-2D bilayer structure of the distribution of hydrogen molecules (indicated by two arrows in the Figure 5 (B)) is formed in **d**=10Å KGO layers, and the distance between two hydrogen molecule layers is in the range of the attractive H_2-H_2 interaction.

Now, we want to examine another aspect of the storage material, namely, the influence of the coverage of the functional group on storage capacity. We calculated the hydrogen storage capacity of KGO for **d**=10Å with different functional group density. Figure 6 shows computational results for the cases of $CO_{0.125}K_{0.063}$, $CO_{0.25}K_{0.125}$, $CO_{0.375}K_{0.188}$, and $CO_{0.5}K_{0.25}$. Since the epoxy and K-epoxy groups increase the magnitude of V_{EFF} (Figure 2), the gravimetric storage capacity increases as the functional group density increases in the low pressure range $(P \leq 2MPa)$. However the isotherms of the KGO at higher pressure show that the storage capacity cannot be in-

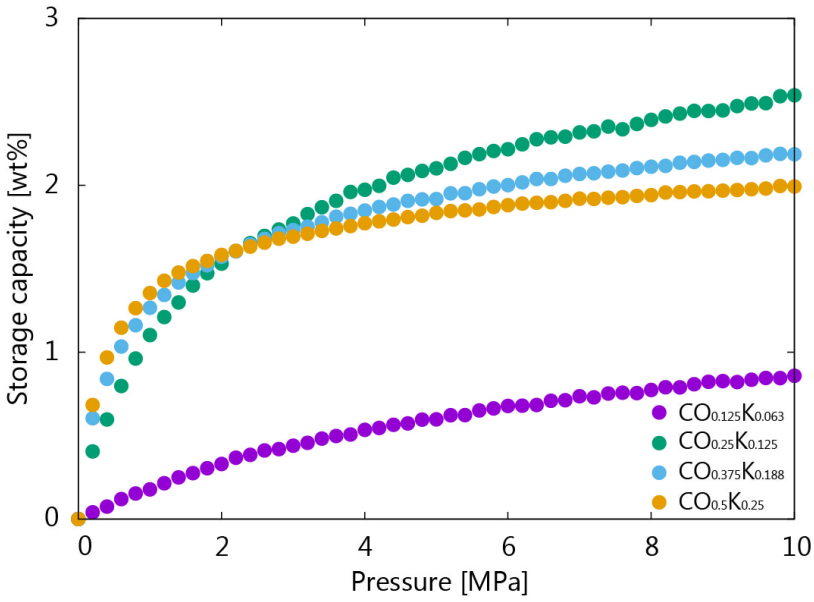

Figure 6: Room temperature storage capacity of KGO with **d**=10 Å for different functional group converages, $CO_{0.125}K_{0.063}$, $CO_{0.25}K_{0.125}$, $CO_{0.375}K_{0.188}$, and $CO_{0.5}K_{0.25}$

creased further by too high functional group coverage. The increase in the weight of the functional group and the expansion of the volume of steric hindrance region are responsible for the decrease of the storage capacity in shown in the figure.

In the GCMC simulations, we calculated the thermodynamic quantities under the classical point particle approximation. In this approximation, we replaced the quantum mechanical partition function ($Q = \sum_n e^{-\frac{E_n}{k_B T}}$) to phase-space integration ($Q = \int exp[-\frac{H(\vec{r}^N,\vec{p}^N)}{k_B T}] d^N\vec{r} d^N\vec{p}$, where $(\vec{r}^N, \vec{p}^N)$ represents the positon and momentum coordiates in the N-particle phase-space) and ignored vibrational-rotational degrees of freedom of the diatomic molecule. The quantum mechanical correction due to the confinement in the

z-direction was considered by directly solving the single particle Schrödinger equation in the z-direction. The PES of the hydrogen molecule inside the KGO of **d**=8Å was used as an example of our quantitative analysis. Our calculation of the partition function for the quantum point particle turned out to be slightly lower (≈3%) than that of the classical point particle, indicating that the classical single particle approximations slightly overestimates the storage capacity. Although vibrational modes are not excited at room temperature due to a large vibrational energy ($h\nu$) compared to k_BT, the zero point energy ($\frac{1}{2}h\nu$) can contribute to the partition function. The calculated vibrational energy of H_2 molecule at the energy minimum position of 4×4 graphene supercell with a potassium-epoxy group (the inset in Figure 2) is 527.5meV, which is 5.5meV lower than that of a free H_2 molecule. The softening of the H_2 vibration mode ($\Delta E_{vib} < 0$) leads to the increase in the partition function inside the KGO by $e^{-\frac{\Delta E_{vib}}{2k_BT}} - 1 \approx 11\%$ at room temperature [36, 25].

In the definition of the PES (Eq. 3.2), we assumed that the direction of the H_2 molecule is fully relaxed, i.e., $E[M+H_2(\vec{r})] \equiv Min_{\hat{\Omega}} E[M+H_2(\vec{r},\hat{\Omega})]$ (where, $\hat{\Omega}(\theta,\phi)$ is the direction of the H_2 molecule, and $E[M+H_2(\vec{r},\hat{\Omega})]$ is the total energy of the storage materials M and the H_2 molecule at position $\vec{r}$ with the direction of $\hat{\Omega}$). In order to account for the decrease of the partition function due to the rotational motion of the H_2 molecule with respect to the direction of the minimum energy, we computed the angle ($\hat{\Omega}$) dependent energy $E[M+H_2(\vec{r},\hat{\Omega})]$ at position $\vec{r_0}$ near the energy minimum position of the same system used in the vibrational motion analysis above and obtained the

angle averaged potential energy $V(\vec{r}_0)_{\hat{\Omega}} = \frac{\int E[M+H_2(\vec{r}_0,\hat{\Omega})] exp\left(-\frac{E[M+H_2(\vec{r}_0,\hat{\Omega})]}{k_B T}\right) d\hat{\Omega}}{\int exp\left(-\frac{E[M+H_2(\vec{r}_0,\hat{\Omega})]}{k_B T}\right) d\hat{\Omega}}$.
The difference between the angle averaged potential and the minimum potential with respect to the rotation angle $\Delta V(\vec{r}_0)_{rot}$ is 2.6meV, so the rotational motion of the H_2 molecule reduces the partition function inside the KGO by $e^{\frac{-\Delta V(\vec{r}_0)_{rot}}{k_B T}} - 1 \approx -10\%$. The net correction to the partition function from above three contributions is $\approx 3\%$(=$0.97 \times 1.11 \times 0.9$) and it means that the single particle assumption of the H_2 molecule in the classical picture is still valid in the context of the storage capacity calculation.

Previously, people attempted to decorate storage materials with various TM atoms, but the clustering of TM atoms posed a serious synthesis problem. The present system is free from metal atom clustering; the K ions are prevented from clustering by the repulsive electrostatic interaction between positively charged potassium ions. Our calculations show that binding energy between the potassium atom and the epoxy group (2.5eV) is larger than the cohesive energy of potassium (1.0eV) and the configuration of separated potassium atoms is more stable than that of aggregated one.

3.4 Summary

In summary, we have proposed a novel hydrogen storage mechanism in the potential well formed inside the void space of porous materials and showed that potassium-intercalated graphite oxide can provide such a void space with a negative potential to realize room temperature hydrogen storage. A relatively uniform potential well is found to be created between the

KGO layer and the origin of the enhanced attractive potential is closely examined. The dependence of hydrogen storage capacity on the interlayer distance and the coverage of functional groups are explained in terms of the effective external potential and the corresponding density enhancement factor.

Chapter 4

Isosteric Heat of Potential Confinement in the Hydrogen Storage Material

In the hydrogen storage problem, if an attractive potential well is formed inside the void space of porous materials, the storage gas density is expected to increase significantly compared to the H_2 gas density outside the material. Actually, the overall H_2 density inside the material is enhanced basically by a Boltzmann factor of $e^{-\frac{U}{k_B T}}$ where $U(<0)$ is some averaged potential energy. Corresponding to this negative potential energy, latent heat is released in the H_2 gas confinement process. We theoretically investigate the energetics involved during the H_2 storage in the potential well and, from the equilibrium thermodynamic principles, we derive a formalism for the isosteric heat of potential confinement of the H_2 gas. Since the gas density inside the potential well increases tremendously, the van der Waals equation is adopted to describe the nonideal gas behavior of H_2. We compare our results to the well-known expression for the isosteric heat of adsorption where, unlike our case, the molecules are bound to specific adsorption sites in the material.

4.1 Introduction

Hydrogen has widely been regarded as a clean and sustainable energy carrier for the future because it does not produce carbon dioxide in burning [1, 2, 37, 38, 39]. Nevertheless, storage of hydrogen in a highly-compressed gas form in existing hydrogen-storage-fuel-cell powered cars (typically at pressure P=700 atm) poses grave concerns about the safety in handling the high-pressure storage tank. There are many proposals to store hydrogen in void spaces in porous materials to reduce the required pressure to within 100 atm. However, in most materials such as metal organic frameworks (MOFs) [40, 41, 42, 43, 44, 45, 46, 4, 47, 48], the magnitude of the adsorption energy is so low that the desirable storage capacity can be achieved only near the liquid nitrogen temperature, which is too low to be practical. If we can confine the H_2 gas inside an attractive potential well, then the density can increase without the necessity of the adsorption of H_2 gas at binding sites. Suppose the inner surface of the voids does not have particular adsorption sites and H_2 molecules rather experience a more or less uniform attractive potential inside the void space. Then H_2 molecules behave like a gas with a relatively free motion inside the well, as opposed to the conventional physisorption localized at specific binding sites on the inner surface. This difference in the storage mode has implications in the energetics of the stored H_2. In the case of the H_2 adsorption in materials such as MOFs or activated carbons [49, 50, 51], there exists a well-established method to experimentally measure the adsorption energy which is called the isosteric heat (enthalpy) of adsorption [52, 53]. In the present study, there should exist

a corresponding quantity because the latent heat is released in the confinement process to a lower-energy state in the potential well. We will derive a formalism to express the change in the enthalpy during the potential confinement in terms of the logarithmic derivative of pressure with respect to temperature in analogy to the isosteric heat of adsorption.

4.2 Isosteric heat of adsorption

In the gas storage by adsorption of the gas molecules in porous materials, the isosteric heat of adsorption is the change in the enthalpy $H(= E + PV)$ of the molecules upon adsorption under the condition of the constant density (number) of the adsorbed molecules. It is well-known that this quantity per mole (ΔH_{st}, the subscript "st" refers to the isosteric condition) is expressed as

$$\Delta H_{st} = R \frac{d \ln P}{d(1/T)}. \tag{4.1}$$

This expression is exact for the adsorption of an ideal gas when the volume occupied by adsorbed molecules is negligibly small, and is reasonably accurate in most practical cases. A latent heat L (> 0 in the present case) is the same as $-\Delta H_{st}$ defined above. It is a common practice that L is obtained, from the two different sets of experimental values (P_1, T_1) and (P_2, T_2) which give the identical number density of the adsorbed molecules (n_{ad}),

$$L = -R\left(\frac{\ln P_2 - \ln P_1}{1/T_2 - 1/T_1}\right)_{n_{ad}} \tag{4.2}$$

For the intended derivation of the isosteric heat of potential confinement, it is a good exercise to follow a derivation in an already known case. For the simplest case of the Langmuir adsorption, the adsorption probability is expressed as, from the two-phase equilibrium thermodynamics [23, **?**],

$$f = \frac{1}{exp[(\varepsilon_{ad} - \mu)/k_B T] + 1} \tag{4.3}$$

Here, ε_{ad} is the energy of H_2 in the adsorbed phase per molecule and μ is the chemical ptoential of H_2 in the gas phase, $\mu = k_B T \ln[(P/k_B T)\lambda^3]$, where $\lambda = (h^2/2\pi m k_B T)^{1/2}$, h is the Planck constant, m is the mass of molecule, and k_B is the Boltzmann constant. Equation 4.3 is also written frequently in the form of $f = P/(P_0 + P)$ [23, 54], where $P_0 = (2\pi m/h^2)^{3/2}$ $\times (k_B T)^{5/2} e^{\varepsilon_{ad}/k_B T}$. (However, readers are warned that adsorption of a real gas on a real surface does not precisely follow the Langmuir equation Equation 4.3).

In the isosteric heat of adsorption measurement, f is a constant and the number of adsorbed molecules $N(= N_{site} f)$ is, by definition, a constant for a given number of adsorption site, N_{site} . Therefore, the variation (δ) of $(\varepsilon_{ad} - \mu)/k_B T$

$$\delta\left(\frac{\varepsilon_{ad}}{k_B T}\right) = \delta\left(\frac{\mu}{k_B T}\right) = \delta(\ln P) - \frac{5}{2}\delta(\ln T). \tag{4.4}$$

We use δ and d (differential in Equation 4.1) interchangeably here because a finite variation is always taken in practical calculations for differentiation. In practice, ε_{ad} may be regarded as independent of temperature, namely, $\delta(\varepsilon_{ad}/k_BT) = (\varepsilon_{ad}/k_B)\delta(1/T)$ and we finally have

$$\varepsilon_{ad} - \frac{5}{2}k_BT = k_B\frac{\delta(\ln P)}{\delta(1/T)} \tag{4.5}$$

The simple relation $\delta(\ln T)/\delta(1/T) = -T$ has been used above. It is possible to interpret the left-hand side of Equation 4.5 as $\Delta h_{st}(= h_{ad} - h_{gas})$, where $h_{ad}(= \varepsilon_{ad} + Pv_{ad})$, enthalpy of the adsrobed molecule) is essentially the same as $\varepsilon_{ad}(< 0)$ with a negligible Pv_{ad} ($v_{ad} = V_{ad}/N$) is the volume per molecule in the adsrobed phase which is much smaller than that in the gas phase) and h_{gas} (enthalpy of the ideal gas) is $\frac{3}{2}k_BT + Pv_{gas} = \frac{5}{2}k_BT$.

4.3 Isosteric heat of potential confinement

Equipped with the experience in the derivation of the isosteric heat of adsorption in a simple case in the previous section, we now proceed to the case of the potential confinement. Even without detailed calculations, we can give a qualitative argument that, the latent heat produced when the hydrogen gas is captured (stored) in the potential well should be almost the same as the magnitude of the potential, $\mid U \mid$. We can also expect that an expression similar to Equation 4.1 would be valid in the present case. A quantitative description starts from the equilibrium condition of the system, $\mu_{in} = \mu_{out}$, where μ_{in} is the chemical potential of the gas inside the potential U and μ_{out} is that outside the storage material where the potential vanishes.

As mentioned before, the density of the H_2 gas inside the potential well increases significantly and it is appropriate to treat it as a non-ideal gas. To describe the high-density H_2 inside the well, we are going to use the van der Waals (vdW) equation of state,

$$(P+\rho^2 a)(1-\rho b) = \rho k_B T \tag{4.6}$$

where the equation is written in terms of the number density $\rho(=N/N)$ for convenience in the derivation presented below. Here, $a = 6.764 \times 10^{-50} Pa \cdot m^6$ and $b = 4.402 \times 10^{-29} m^3$ for H_2 gas [55]. On the other hand, the ideal gas law will be used to describe the low-density H_2 outside the material. We are interested in the relatively low outside pressure range (1-50 atm) in the present study and the deviation of ρ_{out} from the ideal gas for a given P and T is less than 3 % even at 50 atm at room temperature. Parenthetically, we want to note that, if we apply the vdW equation to ρ_{out} as well and follow the same procedure as below, the results look unnecessarily complicated and do not clearly show the simple relation between the isosteric heat and the logarithmic derivative of the pressure with respect to temperature. We will further discuss about this issue later in this section.

From the definition of the isosteric heat of potential confinement, we keep the number of molecules confined in the potential well the same and find the relation between the variation of $\ln P$ and that of temperature. To keep the number of confined molecules unchanged, μ_{in} and μ_{out} continue to be identical. (Otherwise, there would be a change in the number of confined

molecules to make the two chemical potentials identical). Since μ_{in} in the vdW equation is $k_BT\big(\ln[\rho\lambda^3/(1-\rho b)]+\rho b/(1-\rho b)\big)-2\rho a+U$, and μ_{out} within the ideal gas approximation is $k_BT\ln(\rho\lambda^3)$, we have

$$k_BT\big(\ln[\rho_{in}\lambda^3/(1-\rho_{in}b)]+\rho_{in}b/(1-\rho_{in}b\big)-2\rho_{in}a+U=k_BT\ln(\rho\lambda^3). \tag{4.7}$$

For a constant ρ_{in} in this equation, we want the relation between the variation of $\ln P$ and that of T. The term $k_BT\ln\lambda^3$ exists on both sides of the equation and they cancel each other. Dividing Equation 4.7 by k_BT and taking the small variation on both sides, we have, with $\rho_{out}=P/k_BT$ for an ideal gas,

$$\frac{(U-2\rho_{in}a)}{k_B}\delta\big(\frac{1}{T}\big)=\delta\ln\big(\frac{P}{T}\big)=\delta(\ln P)-\delta(\ln T), \tag{4.8}$$

$$U-2\rho_{in}a-k_BT=k\frac{\delta(\ln P)}{\delta(1/T)} \tag{4.9}$$

We have assumed that U is independent of temperature. The kinetic energy $(\frac{3}{2}k_BT)$ exists on both sides of Equation 4.7 and they cancel each other because both sides (in and out) are the gas phase, while in the case of adsorption in Equation 4.5, the kinetic energy for the center of mass motion exists in the gas phase alone and the left-hand side has an additional term of $-\frac{3}{2}k_BT$. The left-hand side of Equation 4.9 may be interpreted as $\Delta h_{st}=h_{in}-h_{out}$, where $U-2\rho_{in}a+\frac{3}{2}k_BT$ and $h_{out}=\frac{5}{2}k_BT$. Again, the volume per molecule in the confined state is much smaller than that of the

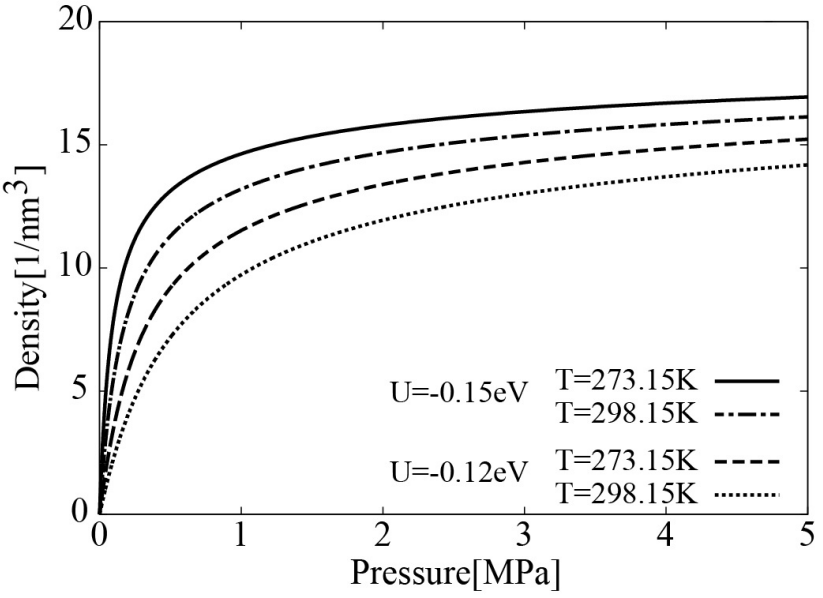

Figure 7: The H_2 storage density inside the potential well (ρ_{in}) as a function of the external pressure (P) up to 5 MPa ($\approx$ 50 atm) at $273.15K$ and $298.15K$. (a) is for the potential strength $U = -0.15eV$ eV and (b) is for $U = -0.12eV$ eV. The higher-density gas inside the well is assumed to be a vdW gas while the lower-density gas outside is an ideal gas.

outside gas and Pv_{in} may be neglected as in Section 4.2. It is interesting to note that the attractive potential contribution ($-2\rho_{in}a$) is reflected in the enthalpy, whereas the hard-wall potential (terms containing the parameter b) which causes the excluded volume effect does not explicitly appear in Equation 4.9. The b term influences the energetics of the vdW gas only indirectly by changing the value of ρ_{in} for the given P and T through Equation 4.7. Effects of rotational and vibrational energies of the H_2 gas are not included in the Δh_{st} calculation. Since H_2 is assumed to have a gas phase both inside and outside the well, the difference in rotational and vibrational

energy between inside and outside the well is expected to be small. It is customary in this research field to plot the isothermal storage density as a function of the outside (externally applied) pressure. In Fig. 1(a) and (b), we plot the isotherms for $U = -0.15eV$ and $U = -0.12eV$, respectively. These potential strengths are typical values required for a room-temperature storage in practical situations. For each U, the storage density is calculated at two different temperatures, $T_1 = 273.15K$ and $T_2 = 298.15K$, chosen for the purpose of room-temperature storage applications. The slopes of the curve decrease as the applied pressure increases due to the H_2-H_2 repulsion term in the vdW equation. With these two isotherms, we can obtain the isosteric heat of potential confinement using Equation 4.9 for a given ρ_{in},

$$\Delta h_{st} \approx k_B \left[\frac{\ln P_2 - \ln P_1}{1/T_2 - 1/T_1} \right]_{\rho_{in}}. \tag{4.10}$$

The results are presented in Fig. 2. The y-coordinate ($-\Delta h_{st}$) is supposed to show $y = |U| + k_B T + 2a\rho_{in}$, linear in ρ_{in} with the slope of $2a$ and crossing the y-axis at $|U| + k_B T$. Both curves are linear in ρ_{in} and their average slope is $6.73 \times 10^{-50} Pa \cdot m^6$ in excellent agreement with the value ($6.764 \times 10^{-50} Pa \cdot m^6$) used in the vdW equation. Furthermore, the crossing points of two curves in Fig. 2 precisely agree with the expected values ($|U| + k_B T$) for $|U| = 0.15eV$ and $0.12eV$ ($k_B T \approx 25meV$ at present), respectively, again confirming the validity of the derived expression.

As mentioned above, the ideal-gas assumption for the outside H_2 is a reasonable approximation, the deviation of which from the real experimental

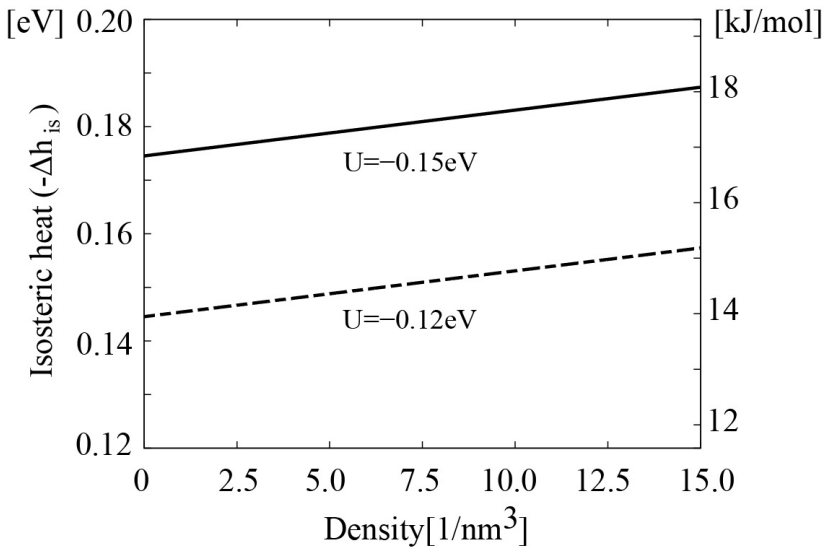

Figure 8: Isosteric heat of potential confinement (Δh_{st}) as a function of ρ_{in} obtained from two isotherms for a given U in Equatino 7. using Equation 4.9. The latent heat ($-\Delta h_{st}$) is plotted as usually done in the literature. We mark the y-axis in terms of both eV/molecule and kJ/mol, where 1eV/molecule = 96.5 kJ/mol.

H_2 density is only within 3% at (the maximum pressure considered here) and still within 6% at pressure as high as 100 atm. It is possible to derive the expression when the outside H_2 gas is described by the vdW equation as well, at the sacrifice of the simplicity and clarity in Equation 4.9. When both inside and outside states are the vdW gas, the resulting equation turns out, after some algebra,

$$U-2(\rho_{in}-\rho_{out})a = k_B\left(\left[1-\frac{\rho_{out}a(1-\rho_{out}-b)}{k_BT}\right]\frac{\delta\ln P}{\delta(1/T)}-\frac{\delta\ln T}{\delta(1/T)}\right)/(1-\rho_{out}b). \tag{4.11}$$

Here, ρ_{out} is of course an implicit function of the outside P through the vdW equation. In the limit of $\rho_{out}a = \rho_{out}b = 0$, Equation 4.11 is reduced to the previous case of Equation 4.9.

4.4 Conclusion

In conclusion, we have considered the room-temperature H_2 storage in the potential well formed inside the material. The H_2 storage capacity is enhanced tremendously, necessitating the non-ideal gas law as exemplified by the vdW equation of state to describe the situation. The isosteric heat of potential confinement is derived for the non-ideal vdW gas in analogy to the isosteric heat of adsorption for the well-known physisorption in porous materials such as MOFs or activated carbons. The results are interpreted in terms of the enthalpy difference of the H_2 gas between inside and outside the potential well.

Chapter 5

Summary

In summary, we theoretically have investigated hydrogen storage in potential well using potassium intercalated graphite oxide (KGO). Firstly, we suggested new storage mechanism based on the diffusive equilibrium of hydrogen gas under the external potential. As a realization of potential well in the nanomaterials, we showed that KGO is good candidate material that accommodates relatively uniform potential well in between successive layers. Potential energy surface is examine by using *ab initio* calculation and the room temperature storage capacity is obtained by performing grand canonical Monte-Carlo simulation. Hydrogen storage capacity for different interlayer distances and functional group densities are explained in terms of density enhancement factor. Secondly, we also explained thermodynamics of confinement process during hydrogen storage. We theoretically investigate the energetics involved during the H_2 storage in the potential well and, from the equilibrium thermodynamic principles, derive a formalism for the isosteric heat of potential confinement of the H_2 gas. We compare our results to the well-known expression for the isosteric heat of adsorption where, unlike our case, the molecules are bound to specific adsorption sites in the material.

Bibliography

[1] L. Schlapbach and A. Züttel, "Hydrogen-storage materials for mobile applications," *Nature*, vol. 414, no. 6861, pp. 353–358, 2001.

[2] B. Sakintuna, F. Lamari-Darkrim, and M. Hirscher, "Metal hydride materials for solid hydrogen storage: a review," *International Journal of Hydrogen Energy*, vol. 32, no. 9, pp. 1121–1140, 2007.

[3] L. J. Murray, M. Dincă, and J. R. Long, "Hydrogen storage in metal–organic frameworks," *Chemical Society Reviews*, vol. 38, no. 5, pp. 1294–1314, 2009.

[4] M. P. Suh, H. J. Park, T. K. Prasad, and D.-W. Lim, "Hydrogen storage in metal–organic frameworks," *Chemical reviews*, vol. 112, no. 2, pp. 782–835, 2011.

[5] M. Dinca, A. Dailly, Y. Liu, C. M. Brown, D. A. Neumann, and J. R. Long, "Hydrogen storage in a microporous metal-organic framework with exposed mn2+ coordination sites," *Journal of the American Chemical Society*, vol. 128, no. 51, pp. 16876–16883, 2006.

[6] E. Durgun, S. Ciraci, W. Zhou, and T. Yildirim, "Transition-metal-ethylene complexes as high-capacity hydrogen-storage media," *Physical review letters*, vol. 97, no. 22, p. 226102, 2006.

[7] G. J. Kubas, "Metal–dihydrogen and σ-bond coordination: the consummate extension of the dewar–chatt–duncanson model for metal–olefin π bonding," *Journal of Organometallic Chemistry*, vol. 635, no. 1, pp. 37–68, 2001.

[8] P. Hohenberg and W. Kohn, "Inhomogeneous electron gas," *Physical review*, vol. 136, no. 3B, p. B864, 1964.

[9] W. Kohn and L. J. Sham, "Self-consistent equations including exchange and correlation effects," *Physical Review*, vol. 140, no. 4A, p. A1133, 1965.

[10] D. C. Langreth and J. P. Perdew, "Exchange-correlation energy of a metallic surface: Wave-vector analysis," *Physical Review B*, vol. 15, no. 6, p. 2884, 1977.

[11] J. P. Perdew, K. Burke, and M. Ernzerhof, "Generalized gradient approximation made simple," *Physical review letters*, vol. 77, no. 18, p. 3865, 1996.

[12] R. P. Feynman, "Forces in molecules," *Physical Review*, vol. 56, no. 4, p. 340, 1939.

[13] D. Hamann, M. Schlüter, and C. Chiang, "Norm-conserving pseudopotentials," *Physical Review Letters*, vol. 43, no. 20, p. 1494, 1979.

[14] L. Kleinman and D. Bylander, "Efficacious form for model pseudopotentials," *Physical Review Letters*, vol. 48, no. 20, p. 1425, 1982.

[15] D. Vanderbilt, "Soft self-consistent pseudopotentials in a generalized eigenvalue formalism," *Physical Review B*, vol. 41, no. 11, p. 7892, 1990.

[16] P. E. Blöchl, "Projector augmented-wave method," *Physical Review B*, vol. 50, no. 24, p. 17953, 1994.

[17] G. Kresse and J. Furthmüller, "Efficient iterative schemes for ab initio total-energy calculations using a plane-wave basis set," *Physical Review B*, vol. 54, no. 16, p. 11169, 1996.

[18] S. Nosé, "A unified formulation of the constant temperature molecular dynamics methods," *The Journal of chemical physics*, vol. 81, no. 1, pp. 511–519, 1984.

[19] W. G. Hoover, "Canonical dynamics: equilibrium phase-space distributions," *Physical Review A*, vol. 31, no. 3, p. 1695, 1985.

[20] W.-Q. Deng, X. Xu, and W. A. Goddard, "New alkali doped pillared carbon materials designed to achieve practical reversible hydrogen storage for transportation," *Physical review letters*, vol. 92, no. 16, p. 166103, 2004.

[21] G. K. Dimitrakakis, E. Tylianakis, and G. E. Froudakis, "Pillared graphene: a new 3-d network nanostructure for enhanced hydrogen storage," *Nano letters*, vol. 8, no. 10, pp. 3166–3170, 2008.

[22] E. Tylianakis, G. M. Psofogiannakis, and G. E. Froudakis, "Li-doped pillared graphene oxide: a graphene-based nanostructured material for hydrogen storage," *The Journal of Physical Chemistry Letters*, vol. 1, no. 16, pp. 2459–2464, 2010.

[23] C. Kittel and H. Kroemer, *Thermal physics*. Macmillan, 1980.

[24] R. S. Aga, C. L. Fu, M. Krčmar, and J. R. Morris, "Theoretical investigation of the effect of graphite interlayer spacing on hydrogen absorption," *Physical Review B*, vol. 76, no. 16, p. 165404, 2007.

[25] S. Patchkovskii, S. T. John, S. N. Yurchenko, L. Zhechkov, T. Heine, and G. Seifert, "Graphene nanostructures as tunable storage media for molecular hydrogen," *Proceedings of the National Academy of Sciences of the United States of America*, vol. 102, no. 30, pp. 10439–10444, 2005.

[26] H.-K. Jeong, Y. P. Lee, R. J. Lahaye, M.-H. Park, K. H. An, I. J. Kim, C.-W. Yang, C. Y. Park, R. S. Ruoff, and Y. H. Lee, "Evidence of graphitic ab stacking order of graphite oxides," *Journal of the American Chemical Society*, vol. 130, no. 4, pp. 1362–1366, 2008.

[27] T. H. Kim, J. Bae, T. H. Lee, J. Hwang, J. H. Jung, K. Sangon, J. S. Lee, D. O. Kim, Y. H. Lee, and J. Ihm, "Room-temperature hydrogen storage via two-dimensional potential well in mesoporous graphite oxide," *preprint*, 2015.

[28] S. Grimme, "Semiempirical gga-type density functional constructed with a long-range dispersion correction," *Journal of computational chemistry*, vol. 27, no. 15, pp. 1787–1799, 2006.

[29] I. F. Silvera and V. V. Goldman, "The isotropic intermolecular potential for h2 and d2 in the solid and gas phases," *The Journal of Chemical Physics*, vol. 69, no. 9, pp. 4209–4213, 1978.

[30] K. A. Mkhoyan, A. W. Contryman, J. Silcox, D. A. Stewart, G. Eda, C. Mattevi, S. Miller, and M. Chhowalla, "Atomic and electronic structure of graphene-oxide," *Nano letters*, vol. 9, no. 3, pp. 1058–1063, 2009.

[31] R. Lahaye, H. Jeong, C. Park, and Y. Lee, "Density functional theory study of graphite oxide for different oxidation levels," *Physical Review B*, vol. 79, no. 12, p. 125435, 2009.

[32] D. W. Boukhvalov and M. I. Katsnelson, "Modeling of graphite oxide," *Journal of the American Chemical Society*, vol. 130, no. 32, pp. 10697–10701, 2008.

[33] M. C. Nguyen, M.-H. Cha, K. Choi, Y. Lee, and J. Ihm, "Calcium-hydroxyl group complex for potential hydrogen storage media: A density functional theory study," *Physical Review B*, vol. 79, no. 23, p. 233408, 2009.

[34] G. Henkelman, A. Arnaldsson, and H. Jónsson, "A fast and robust algorithm for bader decomposition of charge density," *Computational Materials Science*, vol. 36, no. 3, pp. 354–360, 2006.

[35] D. Frenkel and B. Smit, *Understanding molecular simulation: from algorithms to applications*, vol. 1. Academic press, 2001.

[36] C. P. Herrero and R. Ramírez, "Molecular hydrogen in graphite: A path-integral simulation," *Physical Review B*, vol. 82, no. 17, p. 174117, 2010.

[37] A. W. van den Berg and C. O. Areán, "Materials for hydrogen storage: current research trends and perspectives," *Chemical Communications*, no. 6, pp. 668–681, 2008.

[38] M. Z. Jacobson and M. A. Delucchi, "A path to sustainable energy by 2030," *Scientific American*, vol. 301, no. 5, pp. 58–65, 2009.

[39] K. L. Lim, H. Kazemian, Z. Yaakob, and W. W. Daud, "Solid-state materials and methods for hydrogen storage: A critical review," *Chemical engineering & technology*, vol. 33, no. 2, pp. 213–226, 2010.

[40] N. L. Rosi, J. Eckert, M. Eddaoudi, D. T. Vodak, J. Kim, M. O'Keeffe, and O. M. Yaghi, "Hydrogen storage in microporous metal-organic frameworks," *Science*, vol. 300, no. 5622, pp. 1127–1129, 2003.

[41] J. L. Rowsell and O. M. Yaghi, "Strategies for hydrogen storage in metal–organic frameworks," *Angewandte Chemie International Edition*, vol. 44, no. 30, pp. 4670–4679, 2005.

[42] M. Dincă and J. R. Long, "Hydrogen storage in microporous metal–organic frameworks with exposed metal sites," *Angewandte Chemie International Edition*, vol. 47, no. 36, pp. 6766–6779, 2008.

[43] Z. Wang and S. M. Cohen, "Postsynthetic covalent modification of a neutral metal-organic framework," *Journal of the American Chemical Society*, vol. 129, no. 41, pp. 12368–12369, 2007.

[44] K. L. Mulfort, O. K. Farha, C. L. Stern, A. A. Sarjeant, and J. T. Hupp, "Post-synthesis alkoxide formation within metal- organic framework materials: a strategy for incorporating highly coordinatively unsaturated metal ions," *Journal of the American Chemical Society*, vol. 131, no. 11, pp. 3866–3868, 2009.

[45] D. Zhao, D. Yuan, and H.-C. Zhou, "The current status of hydrogen storage in metal–organic frameworks," *Energy & Environmental Science*, vol. 1, no. 2, pp. 222–235, 2008.

[46] H. Furukawa, N. Ko, Y. B. Go, N. Aratani, S. B. Choi, E. Choi, A. Ö. Yazaydin, R. Q. Snurr, M. O'Keeffe, J. Kim, *et al.*, "Ultrahigh porosity in metal-organic frameworks," *Science*, vol. 329, no. 5990, pp. 424–428, 2010.

[47] A. Blomqvist, C. M. Araújo, P. Srepusharawoot, and R. Ahuja, "Li-decorated metal–organic framework 5: a route to achieving a suitable hydrogen storage medium," *Proceedings of the National Academy of Sciences*, vol. 104, no. 51, pp. 20173–20176, 2007.

[48] S. S. Han, J. L. Mendoza-Cortés, and W. A. Goddard Iii, "Recent advances on simulation and theory of hydrogen storage in metal–organic frameworks and covalent organic frameworks," *Chemical Society Reviews*, vol. 38, no. 5, pp. 1460–1476, 2009.

[49] N. Texier-Mandoki, J. Dentzer, T. Piquero, S. Saadallah, P. David, and C. Vix-Guterl, "Hydrogen storage in activated carbon materials: Role of the nanoporous texture," *Carbon*, vol. 42, no. 12–13, pp. 2744 – 2747, 2004.

[50] H. Wang, Q. Gao, and J. Hu, "High hydrogen storage capacity of porous carbons prepared by using activated carbon," *Journal of the American Chemical Society*, vol. 131, no. 20, pp. 7016–7022, 2009.

[51] M. Jordá-Beneyto, F. Suárez-García, D. Lozano-Castelló, D. Cazorla-Amorós, and A. Linares-Solano, "Hydrogen storage on chemically activated carbons and carbon nanomaterials at high pressures," *Carbon*, vol. 45, no. 2, pp. 293–303, 2007.

[52] S. Sircar, R. Mohr, C. Ristic, and M. Rao, "Isosteric heat of adsorption: theory and experiment," *The Journal of Physical Chemistry B*, vol. 103, no. 31, pp. 6539–6546, 1999.

[53] S. Builes, S. I. Sandler, and R. Xiong, "Isosteric heats of gas and liquid adsorption," *Langmuir*, vol. 29, no. 33, pp. 10416–10422, 2013.

[54] R. T. Yang, *Gas separation by adsorption processes*. Butterworth-Heinemann, 2013.

[55] D. R. Lide, "Crc handbook of physics and chemistry," 2001.

[56] W. Gerlach and O. Stern, "Das magnetische moment des silberatoms," *Zeitschrift für Physik A Hadrons and Nuclei*, vol. 9, no. 1, pp. 353–355, 1922.

국문초록

미래의 청정 에너지원인 수소는 연소 시 오염 물질을 발생시키지 않으면서 단위 질량당 연소열이 탄화수소의 약 3배나 된다는 장점을 갖고 있다. 그러나 수소를 안정적이고 효율적으로 저장할 수 있는 방법이 아직 고안되지 않아 일상생활에서 수소를 에너지원으로 사용하는 것은 아직 실현이 되지 못 하였다. 이 문제를 해결하기 위해 본 논문에서는 제일원리 전자구조 계산법과 몬테-카를로 시늉을 통해 수소를 효율적이고 안정적으로 저장할 수 있는 방식을 연구하였고 이를 실현 할 수 있는 흑연으로부터 유도된 나노 물질을 제시하였다.

첫째로, 확산평형에 기반 된 방법을 통하여 상온에서 고밀도의 수소 기체를 포텐셜 우물 안에 가둘 수 있다는 것을 보였다. 만일 수소 기체가 인력을 느낄 수 있는 포텐셜 우물을 만들면, 수소 기체는 그 우물 안에 갖히게 되고, 우물 안에서 분자의 형태를 그대로 유지하게 된다. 이는 이른바 쿠바스 상호작용 이라고 불리는 전이금속과 수소와의 상호작용을 이용하여 수소를 특정 위치 부근에 흡착시키는 것과 크게 다르다. 이 원리를 실험적으로 구현하기 위하여 칼륨 원자가 도입된 산화 흑연을 제시하였고, 산화 흑연의 매 층 사이에 거의 균일한 포텐셜 우물이 형성된다는 것을 밝혔다. 포텐셜의 크기는 대략 0.12eV 정도로, 수소와 저장 물질 사이의 상호작용은 수소와 산화흑연 물질 사이의 반 데르 발스 상호작용과 기능화된 원자들이 만드는 전기장에 의한 수소의 유도 전기쌍극자 상호작용으로 설명 할 수 있다. 상온에서 수소저장량을 계산하기 위하여 몬테-카를로 시늉 계산을 하였다. 저장물질의 화학적 혹은 물리적 성질에 따른 수소저장의 양상을 평형 조건으로 부터 설명하였다.

둘째로, 위와 같은 수소 저장에서 일어나는 열역학적 과정을 설명하였다. 등전자 흡착열은 수소 저장 실험을 설명하는데 있어 가장 중요한 물리량으로 저장 과정에서 수반되는 엔탈피의 변화와 같은 양이다. 이 값을 이론적으로 계산하기 위해서는 수소 기체 사이의 상호작용을 반드시 고려 해야하는데, 무리 전개 방식을 이용하여 수소 기체 사이의 상호작용을 고려하였다. 이를 통해 포텐셜 우물의 깊이 뿐 아니라 수소 기체 사이의 상호작용의 크기가 등전자 흡착열에 반영된다는 사실을 확인하였다. 이 결과는 포텐셜 우물을 이용하여 수소 기체를 저장하는 방식을 이해하는데 도움이 될 것이다.

마지막으로 연구 결과 전체를 간략하게 요약하였다.

주요어 : 수소저장, 흑연, 산화흑연, 기능화기, 포텐셜우물, 밀도증대, 밀도범함수이론, 몬테-카를로시늉

학번 : 2008-20434